Dalton Transactions

Accepted Manuscript

ROYAL SOCIETY OF CHEMISTRY

www.rsc.org/dalton

Journal Name

RSCPublishing

ARTICLE

Investigation of $ZnCo_2O_4$-Pt hybrids with different morphologies towards catalytic CO oxidation

Cite this: DOI: 10.1039/xoxxoooooox

Fan Wang,[a,b] Xiao Wang,[a] Dapeng Liu,[c]* Jiangman Zhen,[a] Junqi Li,[a,b] Hongjie Zhang[a]*

Received ooth January 2012,
Accepted ooth January 2012

DOI: 10.1039/xoxxoooooox

www.rsc.org/

Abstract: In this work, three kinds of $ZnCo_2O_4$ morphologies, that is, rod, plate and sphere, have been successfully prepared and further used to support Pt nanoparticles (NPs) via in situ deposition. The as-prepared $ZnCo_2O_4$-Pt hybrid nanomaterials were then carefully characterized by SEM, TEM, XRD, XPS, ICP EDX, N_2 adsorption measurement in great detail. Besides, the three catalysts were also evaluated by the model reaction of catalytic CO oxidation. After comparing the difference in the three kinds of morphologies, we have tried to clarify the reason for their different catalytic performance. As a result, $ZnCo_2O_4$-Pt sphere was found to be the most active, attaining 100 % CO conversion at a relatively low temperature of 140 °C, because more Pt NPs are prone to distribute on the surface of $ZnCo_2O_4$ sphere than the other ones. The following cycling tests confirm the excellent stability of the as-prepared $ZnCo_2O_4$-Pt samples.

Introduction

Noble metal NPs, especially Pt, have been widely used in various catalytic reactions.[1] As heterogeneous catalyst, the performance of Pt NPs strongly depends on the structure and nature of their supports. The structures with Pt NPs loaded onto the surface of active supports can favour improving the catalytic performance in activity and selectivity for a variety of chemical reactions,[2,3] e.g. for catalytic CO oxidation at low temperatures.[4] Noble metal/metal oxide hybrid catalysts show much promise in heterogeneous catalysis due to possible synergistic effects that occurred between different components.[5-7] Particularly, various Pt/metal oxide systems have been extensively used for catalytic CO oxidation during the past few decades, focusing on the Pt/oxide interface.[8-12] For instance, TiO_2-Pt,[12] Al_2O_3-Pt,[13] CeO_2-Pt,[14] Co_3O_4-Pt[15] and SiO_2-Pt[16] systems have been successfully fabricated. The previous reports have shown that there are some important key factors that affect the catalytic properties. Xia et al. have confirmed that the particles sizes and shapes of noble metals, and the hybrid structures of the final noble metal/metal oxide hybrids can strongly affect the catalytic properties.[17-19] With the fast development of nano-science, more and more efforts have been paid to study the support-effect towards the overall catalytic properties, especially the morphologies of the metal oxides.

Binary metal oxides in a structure of AB_2O_4, where A, B = Ni, Zn, Co, Mn, have been considered as suitable supports to load noble metal NPs owing to their low cost, and richer redox relationship compared with the single component ones.[20-23] Among them, $ZnCo_2O_4$ micro/nano-structures have received more attention and been widely studied.[24-27] Very recently, we have reported that the formation of $ZnCo_2O_4$@CeO_2 core@shell nanostructures showed greatly improved catalytic performance. It is found that the $ZnCo_2O_4$ micro/nano-structures have been successfully prepared with various morphologies, including rods,[26] plates,[28] tubes,[29] wires[30] and spheres[31]. However until now, no morphology-related research has been systematically conducted towards catalytic CO oxidation while $ZnCo_2O_4$ formed hybrids with Pt.

Following the above consideration, three morphologies of $ZnCo_2O_4$, that is rod, plate, and sphere, were synthesized using the hydrothermal route, followed by a self-assembly process to deposit the pre-prepared Pt NPs on the surface of the as-obtained $ZnCo_2O_4$ nanostructures to form the final $ZnCo_2O_4$-Pt hybrids. To elucidate the relationship between morphology and property, the as-obtained $ZnCo_2O_4$-Pt catalysts with different morphology were studied in depth to find the optimal structure with the best catalytic performance on CO oxidation. The role of morphology in CO oxidation behavior of the $ZnCo_2O_4$-Pt catalysts was further discussed according to the analytical results.

Experimental

Preparation of $ZnCo_2O_4$ spheres:[31] In the typical synthesis of $ZnCo_2O_4$ spheres, 2 mmol $Zn(CH_3COOH)_2{\cdot}4H_2O$ and 4 mmol $Co(CH_3COO)_2{\cdot}4H_2O$ were dissolved in 40 mL of ethylene glycol (EG). The mixture was then sealed in a Teflon-lined stainless-steel autoclave and heated to 180 °C and maintained at this for 12 h, then cooled to room temperature. The light green precipitate (ZnCo-glycolate) was collected by centrifugation and washed with ethanol and deionized water for several times, and then was dried in an oven overnight. The as-synthesized ZnCo-glycolate was then annealed at 400 °C for 2 h in air (5 °C min^{-1}) to obtain the $ZnCo_2O_4$ spheres.

Preparation of $ZnCo_2O_4$ plates:[28] In the typical synthesis of $ZnCo_2O_4$ plates, zinc chloride (1 mmol) and cobalt chloride (2 mmol)

were dissolved in 10 mL of distilled water and 10 mL of ethylene glycol and stirred vigorously for 1 h. The resulted slurry was transferred to a 50 mL autoclave, which was then heated to 170 °C and kept overnight. The green precipitates from the autoclave were filtered, washed several times with water, and dried in an oven. Finally, to obtain the porous plates, the precursor was heated to 400 °C and kept for 5 h in air.

Preparation of $ZnCo_2O_4$ rods:[26] In the typical synthesis of $ZnCo_2O_4$ rods, 1 mmol $ZnSO_4{\cdot}7H_2O$ and 2 mmol $CoSO_4{\cdot}7H_2O$ were first dissolved in the mixed solvents composed of 30 mL ethylene glycol (EG) and 10 mL water. Similarly, 3 mmol $H_2C_2O_4$ was added to the identical solutions with the above compositions. The two solutions were slowly mixed together with continuous stirring. Then, the transparent mixture was transferred into an autoclave, which was then tightly sealed and hydrothermally treated at 120 °C for 24 h in an oven. The product was collected by centrifugation and washed with deionized water and absolute ethanol several times and dried in an oven. In the next step, the as-prepared precursor was annealed in air at 500 °C for 2 h at a heating rate of 5 °C min^{-1}.

Synthesis of $ZnCo_2O_4$ supported Pt NPs: 50 mg $ZnCo_2O_4$ spheres/plates/rods and 30mg PVP were first dissolved in 50 mL ethylene glycol. After that, 0.6 mL of 0.02 M K_2PtCl_4 aqueous solution was added into the above solution. Then the mixture was heated to 110 °C and maintained at this temperature for 2 h. The product was collected by centrifugation and washed with deionized water and ethanol several times and dried in an oven.

Characterization: The X-ray diffraction patterns of the products were collected on a Rigaku-D/max 2500 V X-ray diffractometer with $Cu_{K\alpha}$ radiation (λ= 1.5418 Å), with an operation voltage and current maintained at 40 kV and 40 mA. Transmission electron microscopic (TEM) images were obtained with a TECNAI G2 high-resolution transmission electron microscope operating at 200 kV. X-ray photoelectron spectroscopy (XPS) measurements were taken on an ESCALAB-MKII 250 photoelectron spectrometer (VG Co.) with $Al_{K\alpha}$ X-ray radiation as the X-ray source for excitation. Inductively coupled plasma (ICP) analyses were performed with a Varian Liberty 200 spectrophotometer to determine the content. Micromeritics ASAP2020 surface area analyzer was used to measure gas adsorption. The solvent exchanged samples were activated and dried under vacuum at 150 ºC for 15 h. Before measurement, the samples were dried again by using the "outgas" function of the surface area analyzer for 12 hours at 150 ºC to remove all residue solvents in the channels. A sample of about 120 mg was used for N_2 adsorption measurement, and was maintained at 77 K with liquid nitrogen.

Catalytic tests: 30 mg catalysts were put in a stainless steel reaction tube. The CO oxidation tests were performed under conditions in 1 % CO and 20 % O_2 in N_2 at the total flow rate of 30 mL/min. The composition of the gas was monitored on-line by gas chromatography.

Results and discussion

The synthesis procedure of $ZnCo_2O_4$/Pt hybrid nanocatalysts involved two steps. Uniform ZnCo-glycolate nanostructures with different morphologies were first acquired by a hydrothermal method without addition of any surfactant or precipitant,[26, 28, 31] and served as the precursors to produce the $ZnCo_2O_4$ nanostructures. Then the self-assembly process was used to deposit Pt NPs on the surface of the as-obtained $ZnCo_2O_4$ nanostructures to form the final $ZnCo_2O_4$-Pt hybrid nanostructures via an assisted method by adding PVP, ethylene glycol and K_2PtCl_4.

Figure 1 shows the typical SEM images of the as-synthesized ZnCo-precursors and $ZnCo_2O_4$ with different morphologies, which indicates that the synthetic route can result in good yield of rods, plates and spheres.[26, 28, 31] The detailed morphological and structural features of the $ZnCo_2O_4$ powders are also examined by SEM. The as-synthesized ZnCo-precursors exhibit the morphology of 1D rods with diameters of 100-300 nm and lengths on the order of several micrometers, 2D plates with thickness of 40 nm and widths ranging from 100 to 300 nm, 3D spheres with an average diameter of 1-1.5 μm. After heating under air atmosphere, the morphologies well maintain the initial shape of the precursor but become porous.[26, 28, 31] It can be seen that the $ZnCo_2O_4$/Pt products maintain the morphology of 1D rods with diameters of 100-300 nm and lengths of several micrometers and no obvious fragmentation is observed as shown in Figures 2A to 2C. Figures 2 D to 2 F show that the plates are composed of nanosized crystallites with thickness of 40 nm and widths ranging from 100 to 300 nm, while still maintaining the hexagonal morphology. $ZnCo_2O_4$/Pt spheres in Figures 2 G to 2 I are compose of closely packed nanoparticles with diameter of about 10 nm as primary building blocks.

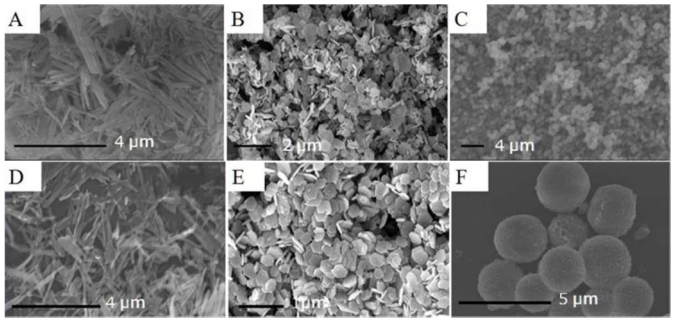

Figure 1. SEM images of A: ZnCo-glycolate rods; B: ZnCo-glycolate plates; C: ZnCo-glycolate spheres; D: $ZnCo_2O_4$ rods; E: $ZnCo_2O_4$ plates; F: $ZnCo_2O_4$ spheres.

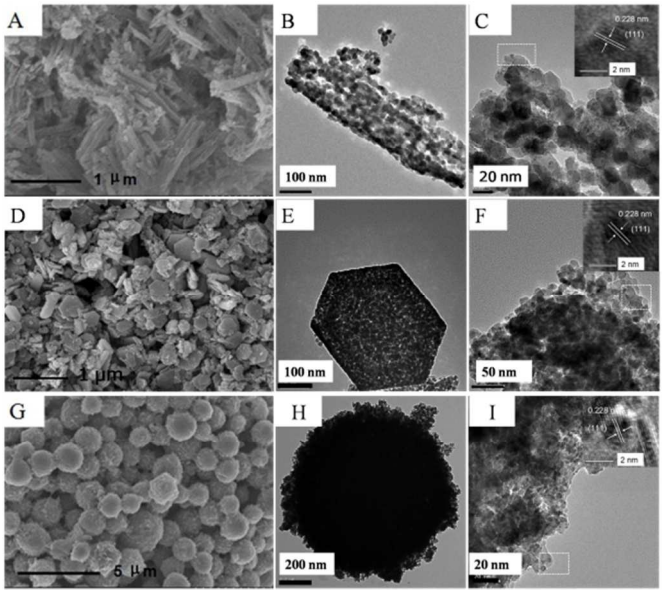

Figure 2. SEM (A, D and G) and corresponding TEM images (others) of A to C: $ZnCo_2O_4$-Pt rods; D to F: $ZnCo_2O_4$-Pt plates; G to I: $ZnCo_2O_4$-Pt spheres.

Then SEM was also used to characterize the deposition of Pt NPs on the $ZnCo_2O_4$ nanostructures. Figure 2 A, 2D and 2 G show that after adding K_2PtCl_4 aqueous solution and refluxed at 110 °C for 2 h, the surface of the $ZnCo_2O_4$ nanostructures began to get rough, indicating the successful surface deposition of Pt components. Figure 2 B, 2 E and 2 H further identify that the final hybrids well maintained their initial morphologies and porous nanostructures. Figure 2 C, 2 F and 2 I show that each $ZnCo_2O_4$ nanostructure is hybridized with hundreds of ultra-small Pt NPs with mean diameter of about 2 nm. The distribution of Pt particle sizes is presented in Figure S1. The mean diameter of Pt particles of rods, plates and spheres are 1.76, 1.88, 1.64 nm, respectively. The clearly observed lattice spacing of 0.228 nm well agreed with that of Pt (111) of 0.227 nm.

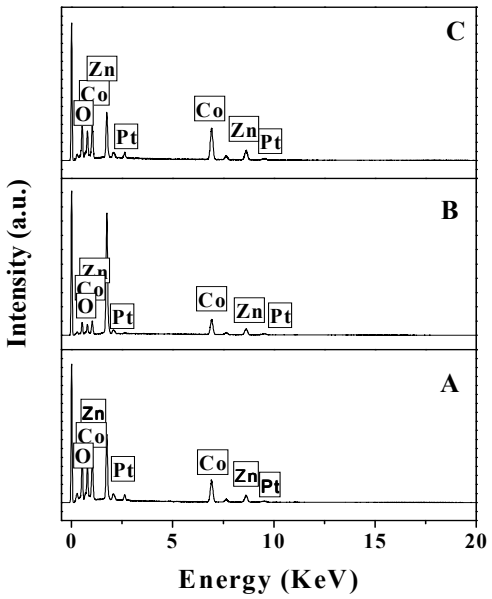

Figure 3. EDX images of (A): $ZnCo_2O_4$ rods, (B): $ZnCo_2O_4$-Pt plates, and (C): $ZnCo_2O_4$-Pt spheres.

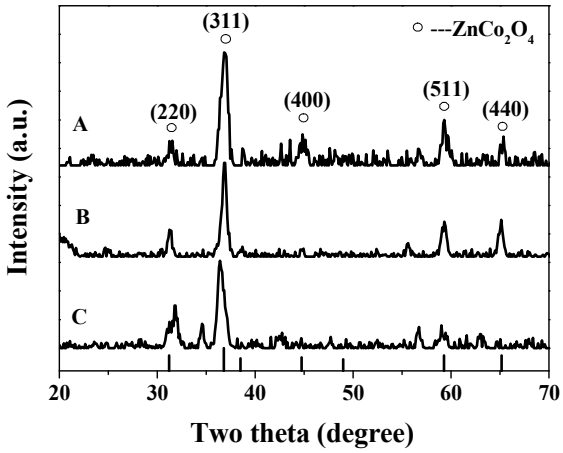

Figure 4. XRD images of (A): $ZnCo_2O_4$-Pt rods; (B): $ZnCo_2O_4$-Pt plates; (C): $ZnCo_2O_4$-Pt spheres.

Energy-dispersive X-ray spectroscopy (EDX) analyses in Figure 3 show that the body of the nanostructures is composed of element Zn, Co, Pt and O. Figure 4 shows the X-ray diffraction (XRD) patterns of the three as-prepared nanocatalysts that the diffraction peaks at 2θ = 31.2º, 36.8º, 44.7º, 59.3º, 65.1º correspond well to the characteristic (220), (311), (400), (511), (440) reflections of spinel-phase $ZnCo_2O_4$, respectively (JCPDS No. 23-1390). No noble metal signal was detected due to low actual content loading on the surface of the $ZnCo_2O_4$ supports, however combined with the EDX results, it could confirm the successful synthesis of $ZnCo_2O_4$-Pt nanostructures. The porosity of the $ZnCo_2O_4$ samples was characterized by N_2 adsorption /desorption isotherm curves as shown in Figure 5. Obviously, the sorption isotherms are of type IV isotherms. They have a distinct H_2-type hysteresis loop in the range of P/P_0 = 0.4-0.99, which does not close until the saturation pressure. The porous structure enhanced the surface-to-volume ratio of the structures. The BET surface areas are 25.1, 39.4, and 20.2 $m^2\ g^{-1}$ for rods, plates and spheres, respectively.

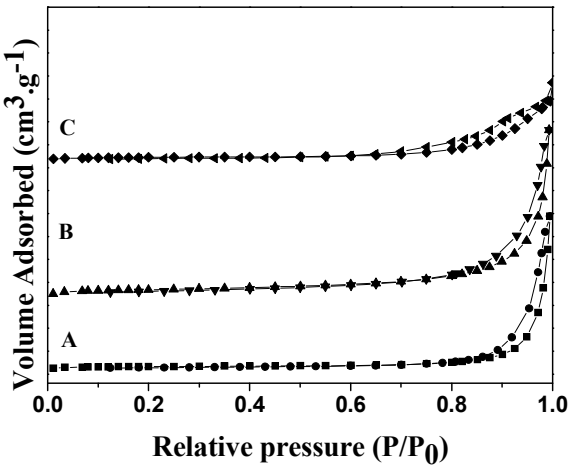

Figure 5. N_2 adsorption-desorption isotherm (A): $ZnCo_2O_4$-Pt rods; (B): $ZnCo_2O_4$-Pt plates; (C): $ZnCo_2O_4$-Pt spheres.

ICP-MS analysis determines that the Pt contents are 1.4 %, 1.8 %, and 1.6 % in molar ratio for $ZnCo_2O_4$-Pt rods, $ZnCo_2O_4$-Pt plates, and $ZnCo_2O_4$-Pt spheres, respectively, as shown in Table 1. The loading of Pt was similar to each other. X-ray photoelectron spectra (XPS) were also employed to examine surface elements and their valence states (Figure 6). The XPS elemental survey scan of the surface of the Pt-loaded $ZnCo_2O_4$ nanostructures reveals that zinc, cobalt, platinum are present in the samples. The XPS curve of Pt 4f was observed at the binding energies of around 71.3 eV (Pt $4f_{7/2}$) and 74.7 eV (Pt $4f_{5/2}$) in good agreement with that in element Pt. The XPS curve of Co 2p shows two major peaks at 795.5 and 780.4 eV, corresponding to the signals of Co^{2+} with Co $2p_{1/2}$ and Co $2p_{3/2}$ spin-orbit, respectively. Two major peaks lying at 1044.4 and 1021.3 eV are characteristic signals of Zn^{2+} with Zn $2p_{3/2}$ and Zn $2p_{1/2}$ orbits, respectively. The full spectrum of XPS was shown to demonstrate that there was no presence of contamination from preparation precursors. The peak integrals of Pt, Zn and Co were calculated from the normalized spectra in Figure S3, and the final data were listed in Table S1. After carefully comparing the integrals of Zn, Co, and Pt peaks, it is found that the relative peak intensity of Pt for $ZnCo_2O_4$-Pt spheres is much stronger than those of $ZnCo_2O_4$-Pt rods and plates. Since the loading Pt amounts are similar in the three samples determined by ICP-MS analysis, Pt NPs tend to obviously distribute more on the surface of $ZnCo_2O_4$-Pt spheres compared with the other two morphologies.

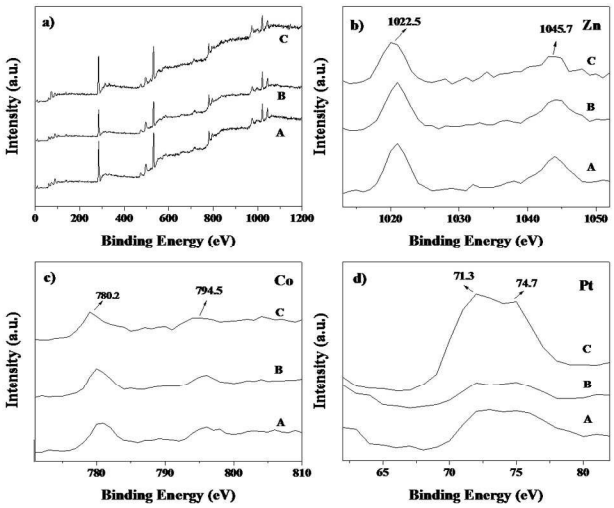

Figure 6. XPS spectra of (A): $ZnCo_2O_4$-Pt rods, (B): $ZnCo_2O_4$-Pt plates and (C): $ZnCo_2O_4$-Pt spheres.

Sample	Pt (ppm)	Zn (ppm)	Co (ppm)	Pt(mol %)	Zn(mol %)	Co(mol %)
rod	37980	341600	483100	1.4	38.5	60.1
plate	41140	241200	448900	1.8	32.2	66
sphere	60150	438100	712100	1.6	35.2	63.2

Table 1. ICP results of $ZnCo_2O_4$ rod, $ZnCo_2O_4$-Pt plate and $ZnCo_2O_4$-Pt sphere.

FTIR was used to characterize the products and the results are shown in Figure 7. The bottommost spectrum is pure PVP, the C=O stretching of PVP is at 1682 cm^{-1}.[32] It was obvious that $ZnCo_2O_4$-Pt with three different morphologies showed a same signal at 1682 cm^{-1}. Although we have dealt the products by washing, there were also PVP residues. This polymer is known to interact with the metal surface through the C=O groups present in its structure,[33-36,40] withdrawing electron density from the metal particles, and therefore affecting their electronic surface state. The amount of PVP surrounding the NPs (and therefore the electronic density of the metal particles) can somehow affecting the catalytic activity of the metal particles, that is why the catalytic performance might decrease in terms of CO conversion.[41-42] So the control experiment was conducted by preparing $ZnCo_2O_4$ supported Pt without adding PVP to rule out the possible influence of PVP. However there were almost no Pt NPs distributed on the surface of $ZnCo_2O_4$ spheres, and it exhibits the same activity as the as-obtained $ZnCo_2O_4$ spheres for catalytic CO oxidation.(Figure S2)

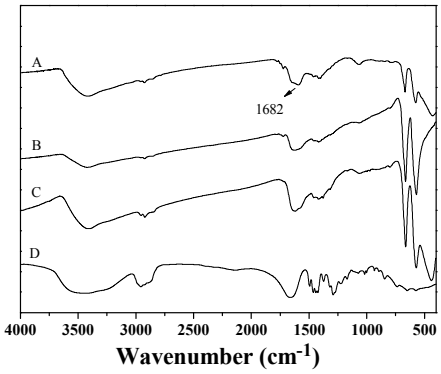

Figure 7. FTIR spectra of (A): $ZnCo_2O_4$-Pt rods, (B): $ZnCo_2O_4$-Pt plates, (C): $ZnCo_2O_4$-Pt spheres and (D): PVP.

As a typical probe reaction to investigate morphology-related effect of $ZnCo_2O_4$-Pt hybrids, CO oxidation is carried out to evaluate the catalytic activities of the three samples of $ZnCo_2O_4$-Pt rods, $ZnCo_2O_4$-Pt plates, and $ZnCo_2O_4$-Pt spheres. In the catalytic process, the gas mixture of CO and O_2 was introduced into the inner space of a stainless steel reaction tube filled up with $ZnCo_2O_4$-Pt catalysts, the surface of which provided the active sites to catalyze CO into CO_2. T_{100}, the temperature for 100 % CO oxidation, is used to compare the catalytic activity of these samples. Figure 8 presents their CO conversion curves that it follows such a sequence of T_{100}: $ZnCo_2O_4$ spheres> $ZnCo_2O_4$ rods > $ZnCo_2O_4$ plates > $ZnCo_2O_4$-Pt rods > $ZnCo_2O_4$-Pt plates > $ZnCo_2O_4$-Pt spheres. As reported the catalytic activities of metal oxides catalysts can be enhanced by forming hybrids with Pt.[3,19] Thus it is reasonably concluded that the enhancement of $ZnCo_2O_4$-Pt nanostructures are probably caused by the similar synergistic effects between $ZnCo_2O_4$ and Pt. Furthermore, if at a constant temperature and O_2 pressure, the steady-state rate, r, of CO_2 formation is recorded as a function of CO pressure, it at first increases continuously with increasing P_{CO}, then reaches a plateau, and finally decreases again. These were observed at temperatures between 450 and 530 K under conditions where the steady-state rate r had just passed the above-mentioned plateau.[37] The Langmuir–Hinshelwood mechanism of the oscillating CO oxidation reaction on

Pt requires adsorption of both reactants, CO and oxygen on the surface.[38-39] It could be proceeded through the following schematic steps:

$$CO + * \rightleftharpoons CO_{ad}, \quad (1)$$

$$O_2 + * \longrightarrow 2O_{ad}, \quad (2)$$

$$CO_{ad} + O_{ad} \longrightarrow CO_{2\,ad}. \quad (3)$$

Obviously all the $ZnCo_2O_4$ catalysts show much lower catalytic activity than the $ZnCo_2O_4$-Pt ones. However, at temperatures lower than 120 ºC, the activity of plate-Pt is higher than the sphere-Pt sample. Based on the previous reports, it is a normal phenomenon that might be caused by different thickness of the shell,[27] different doping element,[47] different sintering temperature,[48] different ratios of O_2 and CO,[49] different contents of the same component,[50] etc. In our case, the phenomenon is supposed to be caused by the twice times larger surface areas of plates than that of spheres. With the increase of temperature, the far lower T_{100} (140 ºC) of $ZnCo_2O_4$-Pt spheres indicates that in our case the optimal structure of $ZnCo_2O_4$ might be spheres. Based on the characterization of TEM, ICP, N_2 adsorption-desorption, FTIR and so on, we can rule out the influence of size and space lattice of Pt NPs, PVP and Cl. Under the observation of N_2 adsorption measurement, XPS results and the ratio of Zn and Co, components and surface areas were regarded as factors. However, the very influential factor is the different dispersion of Pt NPs lead by different morphologies of supports, which dictated the better catalytic property of spheres. In the previous reports,[35, 43-46] different morphologies do affect the properties of catalysts.

Next, a cycling test was performed to study the stability of $ZnCo_2O_4$-Pt spheres (Figure 9). After ten successful cycles from 50 to 150 ºC, $ZnCo_2O_4$-Pt spheres still maintained 100 % conversion of CO into CO_2 at 140 ºC. SEM and XRD (Figure 10) analyses demonstrate that the structure of $ZnCo_2O_4$-Pt spheres remained stable after catalytic cycles. Cycling tests of $ZnCo_2O_4$-Pt rods and $ZnCo_2O_4$-Pt plates were listed in Figure S4 and Figure S5, respectively. After ten successful cycles from 50 to 200 ºC, $ZnCo_2O_4$-Pt rods maintained 100 % conversion of CO into CO_2 at 190 ºC, $ZnCo_2O_4$-Pt plates maintained 100 % conversion of CO into CO_2 at 170 ºC. These results can identify the catalysts were not poisoned by some contaminations.

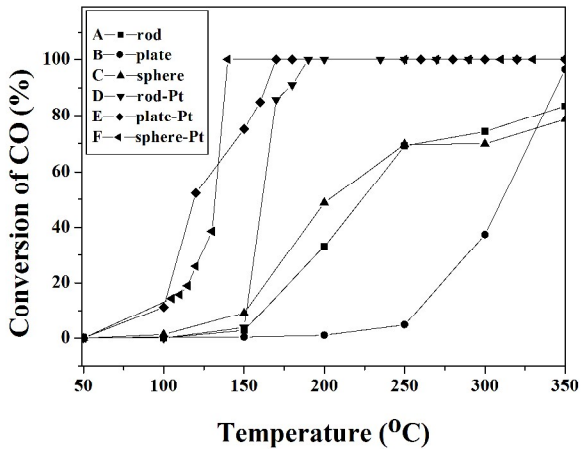

Figure 8. CO conversion curves (A): $ZnCo_2O_4$ rod; (B): $ZnCo_2O_4$ plate; (C): $ZnCo_2O_4$ sphere; (D): $ZnCo_2O_4$-Pt rod; (E): $ZnCo_2O_4$-Pt plate; (F): $ZnCo_2O_4$-Pt sphere.

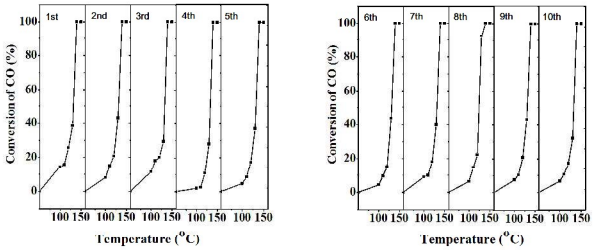

Figure 9. Cycling test of $ZnCo_2O_4$-Pt sphere for CO conversion.

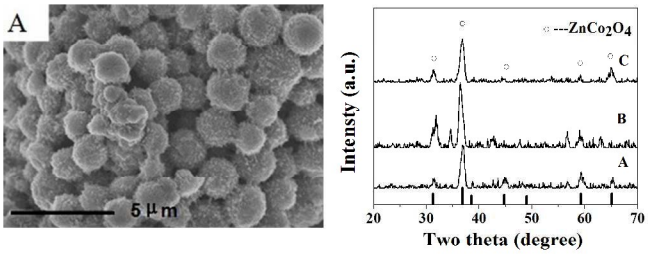

Figure 10. SEM of $ZnCo_2O_4$-Pt sphere (after cycling) and XRD results of: (A): $ZnCo_2O_4$ sphere; (B): $ZnCo_2O_4$-Pt sphere (before cycling); (C): $ZnCo_2O_4$-Pt sphere (after cycling).

Conclusions

In summary, three different morphologies, rods, plates and spheres were synthesized and Pt was deposited on them by the refluxing method. The catalytic properties of the samples have been investigated systematically. All the $ZnCo_2O_4$ nanostructures show much lower catalytic activity than these $ZnCo_2O_4$-Pt nanostructures, which may caused by the suitable decoration amount of Pt nanoparticles and the similar synergistic effects between $ZnCo_2O_4$ and Pt. The determining factor for the differences between these $ZnCo_2O_4$-Pt nanostructures was found to be the effect of different dispersion of Pt NPs. Among the three types of $ZnCo_2O_4$-Pt nanostructures, $ZnCo_2O_4$-Pt sphere was found to exhibit the best catalytic activity, attaining 100 % CO conversion at 140 °C. In addition, it shows a good catalytic stability during the CO oxidation process. It is believed that our $ZnCo_2O_4$-Pt spheres could be a promising candidate catalyst for CO oxidation. Thus, this work supplies an efficient way to optimize the catalytic performance by simply controlling the morphologies, which will surely benefit this kind of catalysts.

Acknowledgements

This work was supported by the financial aid from the National Natural Science Foundation of China (Grant Nos. 91122030, 51272249, 21210001, 21401186, and 21221061), and the MOST of China (Grant No. 2014CB643802).

Notes and references

[a]State Key Laboratory of Rare Earth Resource Utilization, Changchun Institute of Applied Chemistry, Chinese Academy of Sciences, Changchun, 130022 Jilin, China.
[b]Graduate University of Chinese Academy of Sciences, Beijing 100039, P.R. China
[c]Key Laboratory of Bio-Inspired Smart Interfacial Science and Technology of Ministry of Education, School of Chemistry and Environment, Beihang University, Beijing 100191, China.
E-mail: liudp@buaa.edu.cn; hongjie@ciac.ac.cn

Electronic Supplementary Information (ESI) available. See DOI: 10.1039/b000000x/

1 C. Lian, H. Q. Liu, C. Xiao, W. Yang, K. Zhang, Y. Liu and Y. Wang, *Chem. Commun.*, 2012, **48**, 3124.
2 S. Matsumoto, *Catal. Today*, 2004, **90**, 183.
3 X. Wang, D. P. Liu, S. Y. Song and H. J. Zhang, *J. Am. Chem. Soc.*, 2013, **135**, 15864.
4 H. H. Liu, Y. Wang, A. P. Jia, S. Y. Wang, M. F. Luo and J. Q. Lu, *Appl. Surf. Sci.*, 2014, **314**, 725.
5 G. A. Somorjai, J. Y. Park, *Angew. Chem. Int. Ed.*, 2008, **47**, 9212.
6 M. Haruta, N. Yamada, T. Kobayashi and S. Lijima, *J. Catal.*, 1989, **115**, 301.
7 S. J. Tauster, Accounts of Chemical Research, 1987, 20, 389.
8 A. S. Reddy, S. Kim, H. Y. Jeong, S. Jin, K. Qadir, K. Jung, C. H. Jung, J. Y. Yun, J. Y. Cheon, J. M. Yang, S. H. Joo, O. Terasaki and J. Y. Park, *Chem. Commun.*, 2011, **47**, 8412.
9 S. H. Kim, C. H. Jung, N. Sahu, D. Park, J. Y. Yun, H. Ha and J. Y. Park, *Appl. Catal.*, A, 2013, **454**, 53.
10 J. Park, C. Aliaga, J. R. Renzas, H. Lee and G. Somorjai, *Catal. Lett.*, 2009, **129**, 1.
11 J. Y. Park, Y. Zhang, M. Grass, T. Zhang and G. A. Somorjai, *Nano Lett.*, 2008, **8**, 673.
12 K. Qadir, S. H. Kim, S. M. Kim, H. Ha and J. Y. Park, *J. Phys. Chem. C*, 2012, **116**, 24054.
13 M. Meng, P. Y. Lin and Y. L. Fu, *Catal. Lett.*, 1997, **48**, 213.
14 X. Wang, D. P. Liu, S. Y. Song and H. J. Zhang, *Chem. Commun.*, 2012, **48**, 10207.
15 H. X. Zhao, Z. Zheng, J. Li, H. M. Jia, K. W. Wong, Y. D. Zhang and W. M. Lau, *Nano-Micro Lett.*, 2013, **5**, 296.
16 C. H. Jung, J. Yun, K. Qadir, B. Naik, J. Y. Yun and J. Y. Park, *Appl. Catal. B*, 2014, **154**, 171.
17 J. Y. Chen, B. Lim, E. P. Lee and Y. N. Xia, *Nano Today*, 2009, **4**, 81.
18 Y. J. Xiong, H. G. Cai, B. J. Wiley, J. G. Wang, M. J. Kim and Y. N. Xia, *J. Am. Chem. Soc.*, 2007, **129**, 3665.
19 E. Formo, E. Lee, D. Campbell and Y. N. Xia, *Nano Lett.*, 2008, **8**, 668.
20 A. Pendashteh, M. S. Rahmanifar, R. B. Kaner and M. F. Mousavi, *Chem. Commun.*,2014, **50**, 1972.
21 C. Fu, G. Li, D. Luo, X. Huang, J. Zheng and L. Li, *ACS Appl. Mater. Interfaces*, 2014, **6**, 2439.
22 F. Deng, L. Yu, G. Cheng, T, Lin, M. Sun, F. Ye and Y. Li, *J. Power Sources*, 2014, **251**, 202.
23 X. Li, X. B. Zang, Z. Li, X. M. Li, P. X. Li, P. Z. Sun, X. Lee, R. J. Zhang, Z. H. Huang, K. L. Wang, D. H. Wu, F. Y. Kang and H. W. Zhu, *Adv. Funct. Mater.*, 2013, **23**, 4862.
24 Y. Sharma, N. Sharma, G. V. Subba Rao and B. V. R. Chowdari, *Adv. Funct. Mater.*, 2007, **17**, 2855.
25 X. S. Niu, W. P. Du and W. M. Du, *Sensors and Actuators B*, 2004, **99**, 405.
26 Z. G. Jia, D. P. Ren, Q. Z. Wang and R. S. Zhu, *Applied Surface Science*, 2013, **270**, 312.
27 F. Wang, X. Wang, D. P. Liu, J. M. Zhen, J. Q. Li, Y. H. Wang and H. J. Zhang, *ACS Appl. Mater. Interfaces*, 2014, **6**, 22216.
28 Y. C. Qiu, S. H. Yang, H. Deng, L. M. Jin and W. S. Li, *J. Mater. Chem.*, 2010, **20**, 4439.
29 W. Luo, X. L. Hu, Y. M. Sun and Y. H. Huang, *J. Mater. Chem.*, 2012, **22**, 8916.
30 N. Du, Y. F. Yan, H. Zhang, J. X. Yu, C. X. Zhai and D. R. Yang, *Inorg. Chem.*, 2011, **50**, 3320.
31 L. L. Hu, B. H. Qu, C. C. Li, Y. J. Chen, L. Mei, D. N. Lei, L. B. Chen, Q. H. Li and T. H. Wang, *J. Mater. Chem. A*, 2013, **1**, 5596.
32 K. Chan, L. E. Kostun, W. E. Tenhaeff, K. K. Gleason, *polymer*, 2006, **47**, 6941.
33 I. Pastoriza-Santos, L. M. Liz-Marzan, Langmuir 2002, **18**, 2888.
34 H. Tsunoyama, H. Sakurai, Y. Negishi, T. Tsukuda, *J. Am. Chem. Soc.*, 2005, **127**, 9374.
35 L. Chen, Y. Zhang, P. L. Zhu, F. R. Zhou, W. J. Zeng, D. Q. D. Lu, R. Sun, C. P. Rong, Scientific Reports, DOI: 10.1038/srep09672.
36 F. Bonet, V. Delmas, S. Grugeon, R. Herrera Urbina*, P-Y. Silvert, K. Tekaia-Elhsissen, *NanoStruc. Mater.*, 1999, **11**, 1277.
37 G. Ertl, P. R. Norton, J. Rustig, *Phys. Rev. Lett.*, 1982, **49**, 177.
38 Y. Suchorski, W. Drachsel, V. V. Gorodetskii, V. K. Medvedev, H. Weiss, *Surf. Sci.*, 2006, **600**, 1579.
39 R. Imbihl, S. Ladas, G. Ertl, *Surf. Sci.lett.*, 1988, **206**, L903.
40 Y. Borodko, S. E. Habas, M. Koebel, P. Yang, H. Frei, G. A. Somorjai, *J. Phys. Chem. B*, 2006, **110**, 23052.
41 I. Miguel-García, Á. Berenguer-Murcia, D. Cazorla-Amorós, *Appl. Catal. B* 2010, **98**, 161.
42 I. Miguel-Garcíaa, Á. Berenguer-Murciaa, T. Garcíab, D. Cazorla-Amorós, *Catal. Today*, 2012, **187**, 2.
43 B. X. Yuan, W. L. Luan, S. T. Tu, J. Wu, *New J. Chem.*, 2015, **39**, 3571.
44 N. Sutradhar, A. Sinhamahapatra, S. K. Pahari, P. Pal, H. C. Bajaj, I. Mukhopadhyay, A. B. Panda, *J. Phys. Chem. C*, 2011, **115**, 12308.
45 D. W. Gao, A. J. Duan, X. Zhang, Z. Zhao, H. E, J. M. Li, H. Wang, *Appl. Catal. B: Environ.*, 2015, **165**, 269.
46 Z. X. Lin, Y. A. Zhang, Y. Ye, X. T. Zhou, T. L. Guo, *Mater. Technol.*, 2012, **27**, 350.
47 E. Genty, R. Cousin, S. Capelle, C. Gennequin, S. Siffert, *Eur. J. Inorg. Chem.* 2012, **16**, 2802
48 J. L. Cao, Y. Wang, T. Y. Zhang, S. H. Wu, Z. Y. Yuan, *Appl. Catal. B: Environ.*, 2008, **78**, 120.
49 K. Sirichaiprasert, S. Pongstabodee, A. Luengnaruemitchai, *J. Chin. Inst. Chem. Eng.*, 2008, **39**, 597.
50 S. P. Wang, X. Y. Wang, J. Huang, S. M. Zhang, S. R. Wang, S. H. Wu, *Catal. Commun.*, 2007, **8**, 231.

